Available online at www.sciencedirect.com

ScienceDirect

Procedia Materials Science 8 (2015) 218 – 227

Procedia Materials Science

www.elsevier.com/locate/procedia

International Congress of Science and Technology of Metallurgy and Materials, SAM - CONAMET 2013

Microstructural Characteristics of Mold Fluxes Associated to their Thermal Behavior

Edgardo Benavidez[a]*, Elena Brandaleze[a], Leadro Santini[a], Alejandro Martin[a], Constantino Capurro[b], Gonzalo Cerrutti[b], Carlos Cicutti[b]

[a] *Metallurgy Department & Deytema - Facultad Regional San Nicolás (UTN), Colon 332, San Nicolás 2900, Argentina*
[b] *Tenaris R&D, Simini 250, Campana 2804, Argentina*

Abstract

During continuous casting process of steels, several problems can arise when an inadequate heat removal in the mold is produced. This heat extraction occurs through mold powder layers formed between the cooled mold and the solidifying steel. At operating temperatures, the mold flux forms glassy and crystalline phases that affect the heat transfer from the steel to the mold. In this paper, thermal conductivity results, obtained at 900° C, on two commercial mold powders are presented. From these essays, the interfacial thermal resistances: mold/flux and flux/steel were determined. On longitudinal sections of the samples taken from essays, glassy and crystalline phases were characterized. The thermal behavior of these layers is correlated with the proportion of observed phases and chemical composition of each material.

Selection and peer-review under responsibility of the scientific committee of SAM - CONAMET 2013

Mold fluxes; Microstructure; Crystallization; Thermal condcutivity

* Corresponding author. Tel.: +54-336-4420-830; fax: +54-336-4420-820.
E-mail address: ebenavidez@frsn.utn.edu.ar

Selection and peer-review under responsibility of the scientific committee of SAM - CONAMET 2013
doi:10.1016/j.mspro.2015.04.067

1. Introduction

Mold fluxes play an important role during heat extraction from the steel to the continuous casting mold. These materials are poured on the top of the mold and are put in contact with the melt steel. Then, the mold powder is melting and penetrates in the gap formed between the refrigerated copper mold and the solidifying steel shell. The mold flux is fast cooled onto the refrigerated copper wall forming an slag rim that, joining with oscillating of the mould, push the melting flux into the gap. The mold flux penetrates between steel and mold forming three layers: (i) a glassy, (ii) a crystalline, and (iii) a liquid one, Meng and Thomas (2002). To ensure good lubrication, a thin layer of flux remains liquid against the surface (solid) of the steel. The solid layer remains more or less intact and crystallizes throughout the casting process, altering the heat extraction, Nakada et al. (2008). At this stage of the process, heat transfer is controlled by both the thickness and the crystallization degree of the infiltrated powder layers. It is estimated that crystallization of the mold flux presents two effects. On one hand, the crystalline phase produces a greater dispersion of the radiation coming from steel, Susa et al. (1994). On the other hand leads to contraction of the mold powder layer to form an air film (insulator) between the steel and powder, Cho et al. (1998). Both effects lead to increase the total thermal resistance, that is, produce a decrease in the conduction of heat from the steel to the mold.

From the operational point of view, the heat transfer must be controlled to obtain a good quality of the final product and to avoid sticking problems, Kromhout et al. (2002) and Ludlow et al. (2005). During solidification stage, the rate at which heat is removed from the steel depends greatly on the grade of steel to be cast. In medium carbon steels (0.09% -0.16% C) occurs a shrinkage (approximately 4%) due to the transformation δ (austenite) - γ (ferrite), which produces stress that can cause the generation of cracks. These stresses can be minimized by maintaining a thin and uniform solid layer steel (shell). To meet this requirement, heat extraction should be reduced using a thick layer of mod flux with a significant proportion of crystalline phase. On the other hand, the problems of sticking are produced by a poor lubrication between the steel shell and the copper mold. This generally occurs in steels with high carbon content and, in this case, the steel shell formed does not reach to support the ferrostatic pressure. One way to avoid this problem is to form a thicker steel shell by increasing heat extraction. This increase of heat conduction can be achieved by working with a thin and mostly glassy powder layer.

According to previous reports, the extraction of heat from the steel to the mold depends as much of the conduction and radiation mechanisms (emission and absorption) as of the thermal resistances in the zones of contact between powder and molten steel (steel/powder resistance) and between solid powder and copper mold (powder/mold resistance).

In this paper we analyze the microstructure of two layers of commercial mold powders, which have been previously assayed to know their thermal conductivities and thermal resistances developed through mold and steel.

2. Experimental

The chemical composition of the two mold fluxes, named A and B, was determined for different types of analysis including gravimetric, volumetric, spectrophotometric and atomic absorption.

Prior to thermal conductivity testing, both powders were treated at 800 °C (4 hours) to remove carbon from the samples (decarburization). Decarburizing samples showed the following percentage of weight loss: A = 19.1 % and B = 20.9 %.

Decarburized powder was heated to 1300 °C (15 minutes) prior to be poured in the device to determine thermal conductivity. This equipment, whose description has been detailed in previous works, Martín et al. (2007) and Martín et al. (2008), has been used to determine the thermal conductivity -between 700-900 °C- of different mold powders. In this test, based on one developed by Stone and Thomas (1999), the molten powder is poured between a gap of 3 mm in width. This gap is formed by a heated steel plate (hot face) in the one side and a cooled copper mold (cold face) at the other end, simulating real conditions in continuous casting process. On one hand, the steel plate (high temperature) simulates a solid layer of steel, while the copper block cooled by water (low temperature) simulates the continuous casting mold. Temperatures are recorded in five sectors of the device: two in the copper

mold, two in the mold flux and one against the steel plate. The temperature of the steel plate (T_S) is chosen as the test temperature. In this paper, the T_S was maintained between 800-950 °C.

After the thermal conductivity test, flux layers solidified between the steel plate and the mold are extracted. Several sections of such layers (approx. 1 cm in length) were selected to observe the microstructure developed during test. These samples were embedded in resin, polished and etched with nital. The observations of the structure were performed by optical microscopy (Olympus SZ61 and Olympus GX51) and scanning electron microscopy (SEM) in a Philips XL30 CP microscope, the latter with energy dispersive analysis (EDS).

3. Results

3.1. Chemical composition and thermal conductivity of mold fluxes

Chemical composition (wt %) of both powders used in this work is shown in Table 1.

Table 1. Chemical composition of mold powders.

powder	SiO_2	CaO	MgO	Al_2O_3	Fe_2O_3	MnO_2	Na_2O	K_2O	F
A	34.8	27.8	3.12	3.12	0.94	0.04	3.7	0.53	4.98
B	33.9	26.6	2.66	1.20	0.76	0.02	3.6	0.17	2.85

In table 2 are listed the values of heat flux (q), coefficient of thermal conductivity of mold powder (k_P), coefficient of thermal conductivity of the gap or effective (K_{EF}) between steel and mold, and the thermal resistances of interface steel/powder ($R_{S/P}$), powder (R_P) and interface powder/mold ($R_{P/M}$), measure on both powders at 890 ºC ± 10 ºC. The measured values correspond to an average of data which were recorded when the test temperature was held constant for a period of 2-3 minutes.

Table 2. Values measured in the thermal conductivity test.

powder	Q	k_P	k_{EF}	$R_{S/P}$	R_P	$R_{P/M}$
	(MW/m^2)	(W/m.K)	(W/m.K)	(10^{-4} m^2.K/W)	(10^{-4} m^2.K/W)	(10^{-4} m^2.K/W)
A	0.194	2.66	0.73	19.0 (46 %)	11.3 (27 %)	11.1 (27 %)
B	0.209	2.10	0.83	14.6 (40 %)	14.3 (39 %)	7.5 (21 %)

According to the measured values, the total thermal resistance for the flux A: $R_T(A) = 41.4 \times 10^{-4}$ m^2.K/W, and for the flux B: $R_T(B) = 36.3 \times 10^{-4}$ m^2.K/W.

3.2. Optical microscopy

Images of the layers (powders A and B) taken from the thermal conductivity equipment, are showed in Figure 1. According to observations made at low magnification (x15), in both layers can be distinguished that the area near the side of the copper mold presents a glassy phase, whereas the area close to the steel plate presents crystal formation and large number of pores.

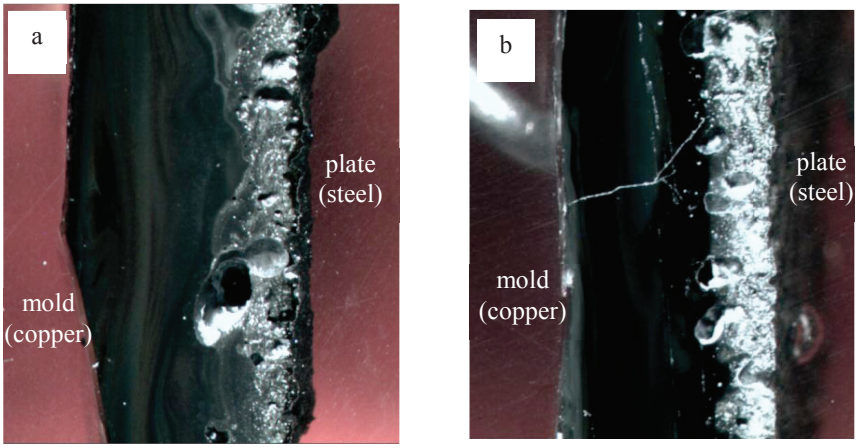

Fig. 1. View of the layers extracted from the heat transfer test: (a) flux A, and (b) flux B.

Observations at higher magnification (x50) allow to distinguish two regions in the crystals (Fig. 2). One of them near to the glassy area, in the middle part of the layer, which has small crystals and the other region closest to the steel plate, which has larger crystals.

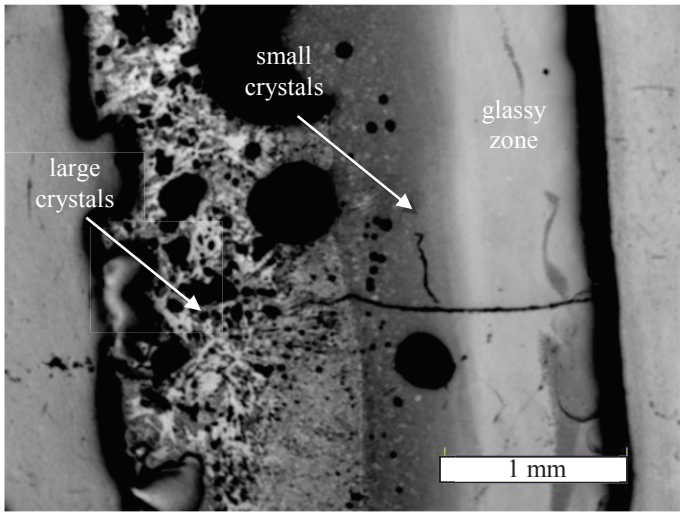

Fig. 2. Typical morphology of the layers extracted from the thermal conductivity test (powder B).

In one sample of each powder was measured the total thickness (L_T) and the width of (i) the zone of large crystals (L_C), (ii) the small crystals or mixed zone (L_M), and the glassy zone (L_G). The values measured (average of several zones) of these layers are shown in Table 3.

Table 3. Thicknesses of the crystalline, mixed, and glassy zones.

flux	L_C (μm)	L_M (μm)	L_G (μm)	L_T (μm)
A	1270 (39%)	1160 (35%)	870 (26%)	3300
B	960 (33 %)	560 (19 %)	1430 (48%)	2950

The percentage of each zone in the total thickness of the layer (L_T) is presented in parentheses. Figure 3 shows the methodology used to measure the different zones.

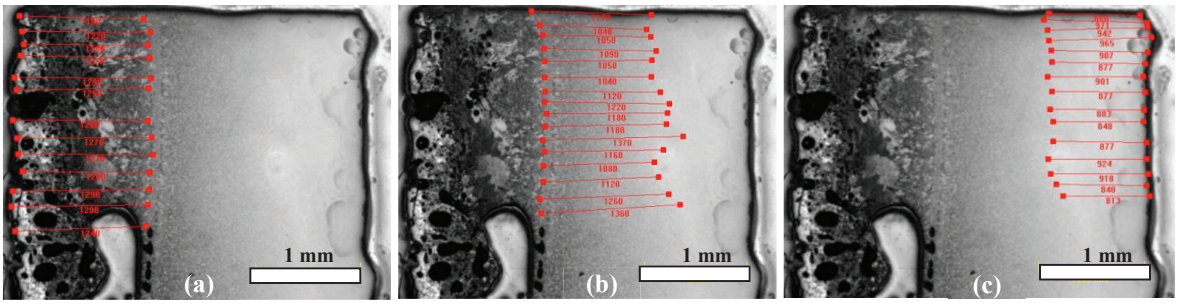

Fig. 3. Determination of the thicknesses of (a) crystalline, (b) mixed, and (c) glassy zones of sample A.

3.3. Electron microscopy

SEM analysis was performed over the entire thickness of the layer to analyze the distribution of oxides and fluorine present in both samples. No changes or trends were detected in the compositions of the different zones analyzed. The average value obtained to each oxide and fluorine across the width of both samples are presented in Table 4.

Table 4. Weight percentage (EDS analysis) of the oxides and fluorine across the width of the layers A and B.

flux	SiO_2	CaO	MgO	Al_2O_3	Fe_2O_3	MnO_2	Na_2O	K_2O	F
A	43.5	39.9	3.91	5.99	1.35	-	3.31	0.85	1.15
B	45.0	39.0	3.88	5.93	1.34	-	3.85	0.38	0.62

In the crystalline zone (closest to the steel plate) can be observed gray dendritic grains with somewhat darker elongated grains (Fig. 4a). Between arms of dendrites highlights a glassy phase (named *matrix*). The EDS analysis of the dendrite and the matrix are listed in Table 5, columns "dendrite" and "matrix 1", respectively.

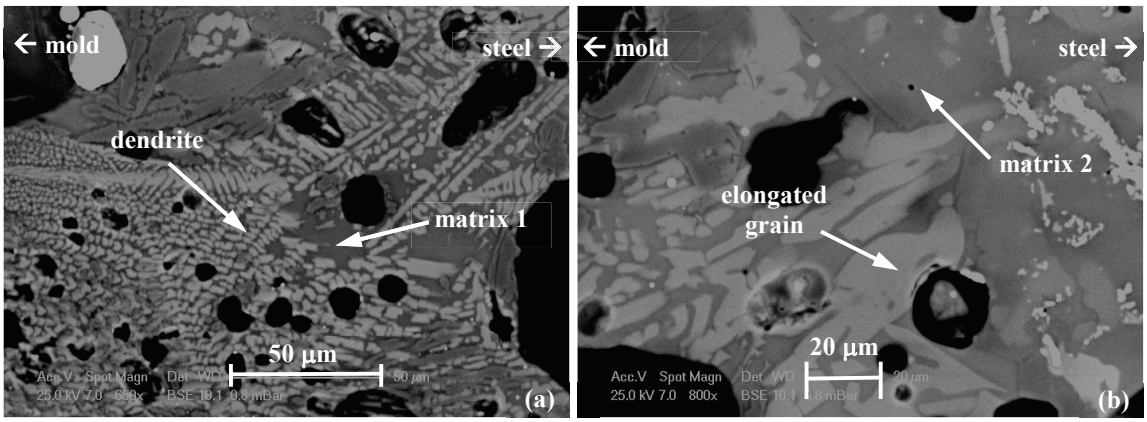

Fig. 4. Micrographs of flux A: (a) dendrites, (b) elongated grains.

A detail of the elongated grains is shown in Figure 4b, where also surrounding amorphous phase (*matrix 2*) is highlights. The EDS analysis (wt %) is listed in Table 5, columns "grain" and "matrix 2".

Table 5. Percentage of oxides and fluorine in crystals and matrix of flux A.

	dendrite	matrix 1	grain	matrix 2
Na_2O	1.86	7.74	1.09	6.90
MgO	2.48	5.06	1.56	6.00
Al_2O_3	3.28	9.71	1.55	9.90
SiO_2	38.8	49.9	34.1	52.7
K_2O	0.50	1.05	0.43	1.20
CaO	48.4	26.6	56.8	23.4
Fe_2O_3	3.05	-	2.65	-
F	1.70	-	1.87	-

Observations on sample B detect a lower presence of dendrites and many elongated grains like "needles" (light gray) in the area near the steel plate (Fig. 5a). Rectangular grains were also observed (dark gray). A detail of both types of grain: elongated (grain 1) and rectangular (grain 2) is presented in Figure 5b.

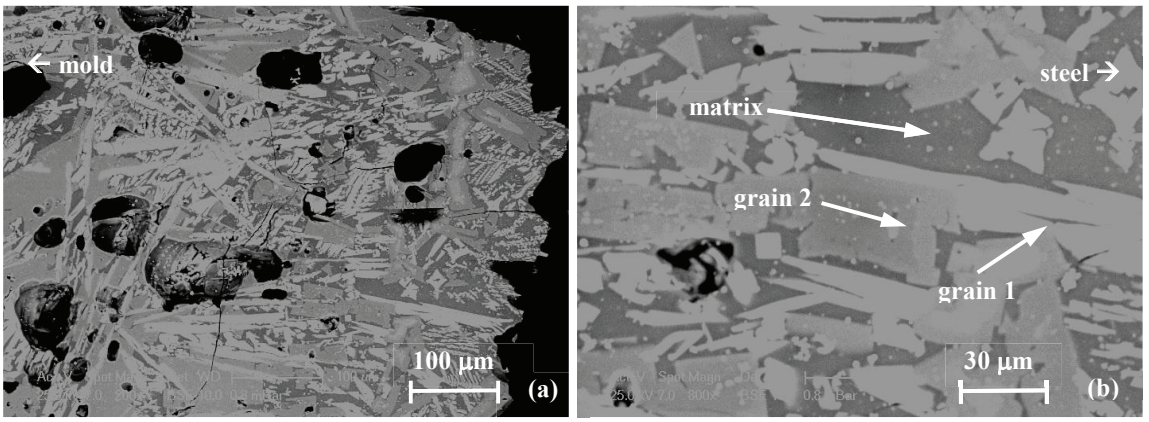

Fig. 5. Micrographs of flux B: (a) area close to the steel, (b) rectangular elongated grains.

The composition (wt %) of the needle and rectangular grains, labeled “grain 1” and “grain 2”, respectively in Fig. 4b, are detailed in Table 6 (column "grain 1" and "grain 2", respectively). This table shows the composition of the glassy phase surrounding grains (column "matrix"), labeled M in Fig. 4b.

Table 6. Percentage of oxides and fluoride crystals and matrix of flux B.

	grain 1 (needle)	grain 2 (rectangular)	matrix (glassy)
Na_2O	2.00	3.31	10.8
MgO	1.76	6.35	4.8
Al_2O_3	2.52	7.75	10.5
SiO_2	36.8	45.1	53.3
K_2O	0.28	0.23	0.68
CaO	53.8	35.2	19.9
Fe_2O_3	1.13	1.81	-
F	1.67	0.26	-

4. Discussion

In Table 7 the percentage of oxides and fluorine of both samples -obtained by EDS analysis (Table 4) and by chemical analysis of the starting powders (Table 1)- is compared. The latter values were modified by considering loss of ignition (the sum of percentage reaches 100%).

Table 7. Comparison of the chemical composition of the powders given by EDS and chemical analysis.

	Powder A		Powder B	
	EDS	chemical	EDS	chemical
SiO_2	43.5	44.0	45.0	47.2
CaO	39.9	35.1	39.0	37.1
MgO	3.91	3.95	3.88	3.71
Al_2O_3	5.99	3.95	5.93	1.67
Na_2O	3.31	4.68	3.85	5.02
K_2O	0.85	0.67	0.38	0.24
Fe_2O_3	1.35	1.19	1.34	1.06
F	1.15	6.30	0.62	3.97
Ca/SiO_2	0.91	0.80	0.87	0.78

By comparing the weight percent determined by both techniques, a good correlation is observed in most of the oxides. The biggest difference is set for Al_2O_3 and fluorine. In the case of Al_2O_3, the values determined by EDS are greater than those reported for chemical analysis, whereas the opposite occurs for fluorine. Because EDS is a semi-quantitative analysis, the values determined by chemical analysis are considered most reliable. Thus, although there are not significant differences in both compositions should be emphasized a higher fluorine and Al_2O_3 contents in the powder A.

Regardless of type of analysis is determined slightly higher basicity in the powder A. According to the measured values, the CaO/SiO_2 ratio is less than 1.0 in both samples, in the powder A = 0.80 and in the powder B = 0.78.

When analyzing crystalline phases of both samples must be considered that during cooling from the melt, powders containing fluorine tend to precipitate cuspidine ($3CaO{\cdot}2SiO_2{\cdot}CaF_2$) as main crystalline phase. According to their molar ratio, cuspidine presents the following distribution: CaO = 45.9 wt%, SiO_2 = 32.8 wt% and CaF_2 = 21.3 wt%. However, in the analysis by EDS fluorine is counted as an element, so that the distribution having the cuspidine (stoichiometric) is: CaO = 58.7 wt%, SiO_2 = 31.4 wt% and F = 9.9 wt%. Considering these values, the composition (EDS) of the so called "grain" (Table 5) and "grain 1" (Table 6) is attributed to the cuspidine. While the percentage of fluorine in these crystals is about 1-2 wt% (according to EDS), remember that EDS underestimates the F content (Table 7). Considering the chemical analysis as a more reliable technique, must be multiply the percentage of fluorine (determined by EDS) by a factor 5.5 for the powder A and by a factor of 6.4 for the powder B. With this setting, the contents of F in both crystalline phases (grain and grain 1), are about 10 wt%, which is in agreement with the contents of F (9.9 wt%) for the cuspidine.

Dendrites analyzed in the powder A (Table 5) have a composition close to the stoichiometric cuspidine with lower percentages of CaO but higher in SiO_2. However, it could also correspond to cuspidine phase (with non-stoichiometric composition). The non-stoichiometry can be justified if one considers that this area of the sample has undergone a high cooling rate. In this case, cuspidine crystals -with the ratio: CaO: SiO_2 : CaF_2 = 3: 2: 1- would not be achieved to form.

Based on the starting composition, Ryu et al. (2010) examined how the binary basicity (CaO/SiO_2 = Bi), and the Al_2O_3 content affect the crystallization behavior of three slags. The authors note that the heat flux and the thickness of the powder layer decrease with increasing the basicity and the content of Al_2O_3. In other work, Tang et al. (2008) investigated the influence on the heat flux of: (i) the content of F, (ii) the binary basicity (CaO/SiO_2) and (iii) the cooling water rate. They selected 1400 °C as working temperature obtaining layers of 1-5 mm in thickness. The authors note that by increasing the content of F (from 2 wt% to 10 wt%), the heat flux (q) through the powder layer decreases. Although the thickness of the solid layer also decreases with increasing F (greater q), the influence of the percentage of crystalline phase is the dominant factor. This behavior is attributed to that the F^- can replace O_2 in the Si-O bond (acting as network modifier), which favors the precipitation of crystals in the melt. Thus, the authors

focus on recrystallization of the powder as an important factor influencing on the heat flux. In such work, it is observed that increasing the binary basicity (up to 1.4) the heat flux decreases.

According to these papers, in the present work the powder A should present a lower heat flux than powder B, because it has: (i) higher content of fluorine, (ii) higher content of Al_2O_3 and (iii) greater ratio CaO/SiO_2.

From values obtained in the test of heat transfer, and in accordance with the above, the powder A presented a lower heat flow (Table 2). The behavior of the powder B is associated with both a higher effective thermal conductivity and a lower thermal resistances on both interfaces.

The effective thermal conductivity (K_{EF}) determined at 890 °C for both powders was compared to the known K_{SYS}, which can be calculated from the chemical composition of the starting powder, Holzhauser et al. (1999). The K_{SYS} values were obtained for 1200 °C and 1300 °C and then extrapolating to the temperature of interest (890 °C). The values obtained were: K_{SYS} (A) = 0.80 W/mK and K_{SYS} (B) = 0.84 W/mK, which is a good agreement with the measured values (less than 10% differences). In both powders, the thermal resistance in the steel-powder interface ($R_{S/P}$) is greater than the thermal resistance in the powder-mold interface ($R_{P/M}$). This fact is attributed to the flux contraction when the crystallization is produced in the area close to the steel plate (Fig. 1). This contraction produces a thin layer of air which increases the thermal resistance between the steel and the mold flux. In the zone near the cooled copper mold, the formation of a glassy layer is observed in both samples. This non-crystalline layer did not cause significant contraction against copper wall, so the thermal resistance $R_{P/M}$ is lesser than $R_{S/P}$.

Thermal resistance study has also been developed by Cho et al. (1998), who conclude that the interfacial thermal resistance increases with increasing the thickness of the mold flux layer. They also report that the steel-powder interfacial resistance contributes about 50% of the total thermal resistance, in agreement with the values reported in the present study (40-50%).

The structure of both tested samples exhibit pores, whose presence may be due to the shrinkage during cooling and/or the removal of gaseous phases. Moreover, in the microstructure developed in both samples, the zone facing the copper mold (cold side) shows a glassy phase, then a zone of small crystals (called mixed layer), and then a layer showing large elongated and rectangular crystals is developed against the steel plate (hot face). On the other hand, sample A has a higher proportion of fine dendrites in the intermediate/mixed layer.

Analyzing the temperature profile throughout the thickness of the layers it is observed that the region where they develop larger crystals (thickness L_C) is between 900-600 °C for the powder A and between 900-650 °C for powder B. While the mixed zone of small crystals (thickness L_M) is developed for temperatures between 600-450 °C (powder A) and 650-550 °C (powder B). Mizuno et al. (2008) report that, for powders with 7 wt% F, the maximum rate of grain growth is achieved at T ~ 800C and the maximum rate of nucleation at T ~ 600C. They note that cuspidine is the only crystalline phase developed, and to T ≤ 520 °C no crystal formation is detected. Although during the thermal conductivity test, molten fluxes solidified with different thermal gradients, the temperature regions associated with each morphology are in good agreement with those reported by Mizuno et al. (2008).

In thermal conductivity tests, the powders A and B (melted at 1300 °C) show a fast cooling up to the measurement temperature (~ 950 °C). Therefore, crystals formation is expected before recording of the conductivity values. Thus, according to the TTT diagram developed by Kashiwaya, Cicutti and Cramb (1998), during solidification, first crystalline formation is dicalcium silicate ($2CaO{\cdot}SiO_2$) and then, below 1050 °C, the cuspidine formation is dominant. Although in this study have not been made cooling curves, it is expected that the main crystal formation is developed prior to the beginning of the thermal conductivity test (at T ~ 890 °C). In the present work, probably the first phase to crystallize is wollastonite ($CaO{\cdot}SiO_2$) according to the composition of the rectangular grains present (post-test) in the layer of powder B ("grain 2" in Fig. 5b), and as it is also reported by Nakada et al. (2005). In the mentioned work the "nose" of the cuspidine crystallization (TTT curve corresponding to a synthetic mold powder) is presented around 880 °C, while the nose of the wollastonite formation occurs above 1000 °C. Besides, the authors noted that the rate of cuspidine crystallization is considerably higher than to the wollastonite and they reported a greater proportion of dendritic crystals when the basicity of mold powder increased.

In this way, the different zones observed in mold flux layers extracted from the conductivity test, could be explained by the rates of nucleation and growth of crystals. Thus, the zone of fine crystals (intermediate/mixed zone) has small crystals (main phase: cuspidine) because they have undergone a high cooling rate from the melt

(1300 °C) to a temperature where the nucleation rate is high and the rate of growth is low, resulting in a structure with a large number of small crystals. Probably due to the high cooling rate suffered by this zone the wollastonite-type phase was not developed to a great extent. Furthermore, the area closest to the steel plate (hot side) suffered a slower cooling rate from melt to a temperature where the growth rate is higher than the nucleation rate, resulting in a lower amount of larger crystals, Ryu etal. (2010). In this case, the lowest cooling rate would result in the formation of crystals type $CaO{\cdot}SiO_2$. Obviously, the glassy layer forms against the copper wall (cold side) because the cooling rate is so high that there is not enough time for the formation of crystals.

Finally, according to the greater thickness of the crystal layer of powder A, higher thermal resistance is expected from this powder. Cho et al. [4] gives an expression for calculating the interfacial thermal resistance steel/powder (R_{INT}) in accordance with the thickness of the crystal layer (d_{CRY}), according to equation (1):

$$R_{INT}(10^{-4} m^2 K/W) = 16.4 \cdot d_{CRY}(mm) \quad (1)$$

Taking the values of L_C from Table 3 and replacing in d_{CRY} of Eq. (1), then the interfacial resistances of both fluxes are: R_{INT} (A) = 20.8 · 10^{-4} m^2.K/W and R_{INT} (B) = 15.7 · 10^{-4} m^2.K/W. These values are within 10 % of difference to the resistances $R_{S/P}$ measured in both powders (Table 2).

5. Conclusions

The values of the heat flux (q) and the coefficient of effective thermal conductivity (K_{EF}), measured around 900 °C in two commercial mold powders (A and B) were linked to the starting chemical composition. The lower heat conduction presented by powder A was attributed to the higher fluorine content, higher percentage of Al_2O_3 and higher ratio CaO/SiO_2 respect to powder B. These characteristics promote a higher degree of crystallization in the powder A, which is shown in this paper through the greatest ratio crystalline/glassy phases presents in this powder. Associated with this behavior of largest percentage of crystals in the powder A, higher thermal resistance at the interface steel/powder of such material is presented.

In the crystalline zone of both materials are observed two regions differentiated by the grain size. This microstructure was interpreted based on the cooling rates that experienced the different zones of both powders and the thermal gradient imposed during the thermal conductivity test. The middle zone has small dendrites, here the cooling rate favors the cuspidine formation ($3CaO{\cdot}2SiO_2{\cdot}CaF_2$) because this phase has a high crystallization rate. That zone is located in a region of temperatures where the rate of nucleation is greater than the grain growth, justifying the presence of small crystals. Furthermore, in the area close to the steel plate, elongated grains of cuspidine and rectangular crystals of wollastonite ($CaO{\cdot}SiO_2$) are present. In this zone of higher temperature, the growth rate is higher than the nucleation one promoting the formation of larger crystals. Furthermore, a lower cooling rate allows precipitation of aluminosilicate phases as wollastonite, which have a lower crystallization rate than cuspidine.

Finally, it is emphasize that both the effective thermal conductivity (K_{EF}) and the steel/powder interfacial thermal resistance ($R_{S/P}$) were in good agreement with the models proposed in previous works. The K_{EF} was compared with the thermal conductivity calculated from the starting chemical composition, while ($R_{S/P}$) was compared with the interfacial thermal resistance which takes into account the thickness of the crystal layer. In both cases the differences were less than 10%.

Acknowledgements

The authors wish to thank the Universidad Tecnológica Nacional and TENARIS for the financial support provided to this project.

References

Cho, J., Shibata, H., Emi, T., Suzuki, M., 1998. Thermal resistance at the interface between mold flux film and mold for continuous casting of steels. ISIJ International 38, 440-446.

Holzhauser, J.F., Spitzer, K.H., Schwerdtfeger, K., 1999. Study of heat transfer through layers of casting flux: experiments with a laboratory set-up simulating the conditions in continuous casting. Steel Research 70, 252-258.

Kashiwaya, Y., Cicutti, C., Cramb, A., 1998. An investigation of the crystallization of a continuous casting mold slag using the single hot thermocouple technique. ISIJ International 38, 357-265.

Kromhout, J.A., Ludlow, V., McKay, S., Normanton, A.S., Thalhammer, M., Ors, F., Cimarelli, T, 2002. Physical properties of mould powders for slab casting. Ironmaking and Steelmaking 29, 191-193.

Ludlow, V., Harris, B., Riaz, S., Normanton, A., 2005. Continuous casting mould powder and casting process interaction: why powders do not always work as expected. Ironmaking and Steelmaking 32, 120-126.

Martín A., Benavidez E., Santini L., Brandaleze E., 2007. Determinación de transferencia térmica a través de capas de polvo colador fundido, Proceedings Congreso SAM/CONAMET, San Nicolás, Argentina, 1552-1557. (In Spanish).

Martín, A., Brandaleze, E., Benavidez, E., Santini, L., Di Gresia, G., 2008. Desarrollo de un equipo para medición de conductividad térmica en polvos coladores fundidos, Proceedings 39th Steelmaking Seminar Internacional, Curitiba, Brazil, 439-446. (In Spanish).

Meng, Y., Thomas, B.G., 2003. Interfacial friction related phenomena in continuous casting with mold slags, ISSTech 2003 Conference Proceedings, Indianapolis, USA, p. 589-606.

Mizuno, H., Esaka, H., Shinozuka, K., Tamura, M., 2008. Analysis of the crystallization of mold flux continuous casting of steel. ISIJ International 48, 277-285.

Nakada, H., Susa, M., Seko, Y., Hayashi, M., Nagata, K., 2008. Mechanism of heat transfer reduction by crystallization of mold flux for CC. ISIJ International 48, 446-453.

Nakada, H., Watanabe, T., Nagata, K., 2005. Heat transfer through slag film with crystalline layer, ICS Proceedings, 787-793.

Ryu, H.G, Zhang, Z.T., Cho, J.W., Wen, G.H., Sridhar, S., 2010. Crystallization behaviors of slags through a heat flux simulator. ISIJ International 50, 1142-1150.

Stone D.T., Thomas B.G., 1999. Measurement and modeling of heat transfer across interfacial mold flux layers. Canadian Metallurgical Quaterly 38, 363-375.

Susa, M., Mills, K.C., Richardson, M.J., Taylor, R., Stewart, D., 1994. Thermal properties of slags films taken from continuous casting mould. Ironmaking and Steelmaking 21, 279-286.

Tang, P., Xu, C., Wen, G., Zhao, Y., Qi, X., 2008. Heat flux through slag film and its crystallization behavior. J. Iron & Steel Research International 15, 7-11,20.